

# Rolling quantum dice with a superconducting qubit

R. Barends,<sup>1,\*</sup> J. Kelly,<sup>1,\*</sup> A. Veitia,<sup>2</sup> A. Megrant,<sup>1</sup> A. G. Fowler,<sup>1,3</sup> B. Campbell,<sup>1</sup> Y. Chen,<sup>1</sup> Z. Chen,<sup>1</sup> B. Chiaro,<sup>1</sup> A. Dunsworth,<sup>1</sup> I.-C. Hoi,<sup>1</sup> E. Jeffrey,<sup>1</sup> C. Neill,<sup>1</sup> P. J. J. O'Malley,<sup>1</sup> J. Mutus,<sup>1</sup> C. Quintana,<sup>1</sup> P. Roushan,<sup>1</sup> D. Sank,<sup>1</sup> J. Wenner,<sup>1</sup> T. C. White,<sup>1</sup> A. N. Korotkov,<sup>2</sup> A. N. Cleland,<sup>1</sup> and John M. Martinis<sup>1</sup>

<sup>1</sup>*Department of Physics, University of California, Santa Barbara, CA 93106, USA*

<sup>2</sup>*Department of Electrical Engineering, University of California, Riverside, CA 92521, USA*

<sup>3</sup>*Centre for Quantum Computation and Communication Technology,  
School of Physics, The University of Melbourne, Victoria 3010, Australia*

(Dated: June 16, 2014)

One of the key challenges in quantum information is coherently manipulating the quantum state. However, it is an outstanding question whether control can be realized with low error. Only gates from the Clifford group – containing  $\pi$ ,  $\pi/2$ , and Hadamard gates – have been characterized with high accuracy. Here, we show how the Platonic solids enable implementing and characterizing larger gate sets. We find that all gates can be implemented with low error. The results fundamentally imply arbitrary manipulation of the quantum state can be realized with high precision, providing new practical possibilities for designing efficient quantum algorithms.

The Platonic solids have been studied since ancient times for their beauty and symmetry [1], and make excellent random number generators [2]. Here, we exploit their symmetry for quantum information. Quantum processing would benefit from having a large set of accurate gates to reduce gate count and error [3–5], yet it is an open question whether arbitrary gates can be implemented with low error – only the restricted group of Clifford gates [6, 7] has been used with high precision [8–10]. We use the Platonic solids as a pathway and implement gate sets inspired by the tetrahedron, octahedron, and icosahedron, including gates never previously benchmarked. We achieve low error for all gates. These results illustrate the potential of using unitaries with a fine distribution, and suggest arbitrary rotations can be realized with high accuracy, opening new avenues for performing gates and designing algorithms efficiently.

Recently, major advances have been made in accurately implementing octahedral (Clifford) gates on a variety of platforms. Superconducting qubits, liquid NMR and ion traps have shown single-qubit gate errors ranging from  $10^{-3}$  to  $10^{-6}$  [8–10], determined via Clifford-based randomized benchmarking (RB). However, process verification of non-Clifford gates is a conundrum: Quantum process tomography can be used, but state preparation and measurement error can lead to significant systematic deviations, limiting precision. Clifford-based RB is insensitive to these errors, but unavailable for gates which fall outside of the Clifford group. Here, the use of other rotational groups allows for randomized benchmarking of non-Clifford gates. A different approach to estimating errors of non-Cliffords was proposed in Ref. [11].

The groups of unitaries we use here are formed by the rotations that preserve the regular tetrahedron, octahedron, and icosahedron – Platonic solids – in the Bloch sphere representation, see Fig. 1. These are the rotational subgroups of the tetrahedral, octahedral and icosahedral symmetry groups  $T_h$ ,  $O_h$  and  $I_h$ . These ro-

tations exchange faces, amounting to a quantum version of rolling dice (such dice are referred to as d4, d8, and d20), but now in Bloch space. The tetrahedral, octahedral and icosahedral rotational groups have size (order) 12, 24, and 60, respectively. The axes are defined by the lines that intersect the origin, and a face center, vertex, or midpoint of an edge. The angles of rotation around these axes are, respectively, integer multiples of  $\{2\pi/3, 2\pi/3, \pi\}$  for the tetrahedral group,  $\{2\pi/3, 2\pi/4, \pi\}$  for the octahedral group, and  $\{2\pi/3, 2\pi/5, \pi\}$  for the icosahedral group. The tetrahedral rotations (orange axes in Fig. 1) are shared among all three groups, enabling comparison experiments. The octahedral rotations form the single-qubit Clifford group. The icosahedral rotations form the most dense group – the icosahedron is the largest of the Platonic solids – allowing for fine unitary control.

For implementing gates from these groups we decompose them into rotations around the X, Y, and Z

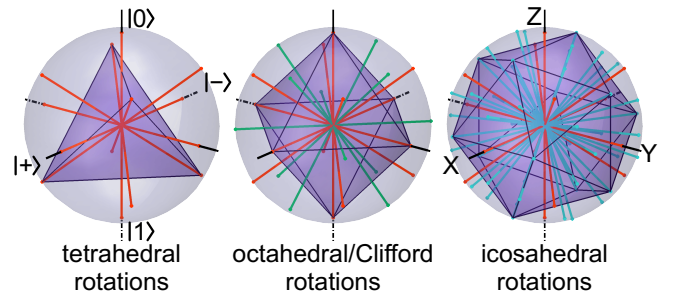


**FIG. 1: The Platonic solids and their rotational groups.** The axes of rotation are of the tetra-, octa- and icosahedral rotational group; the respective Platonic solids are superimposed. The axes are defined by lines intersecting the origin, and a vertex, face center, or midpoint of an edge. The tetrahedral rotational group (orange) is shared among all groups.

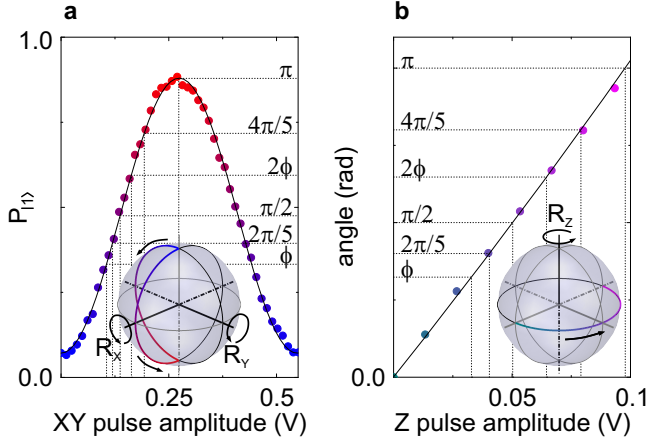


FIG. 2: **Calibrating the angles of rotation.** (a) The excited state probability versus X and Y pulse voltage amplitude on the control board. The amplitudes for the required phases of rotations around the X and Y axes are indicated with dotted lines. The data follow a  $\sin^2$  dependence (solid line) on the pulse amplitude, as expected. Data not corrected for measurement fidelity. (b) The phase of the quantum state as a function of Z pulse voltage amplitude, measured using quantum state tomography. Solid line is a fit to the data. For brevity, only the positive angles are shown. Here  $\tan \phi = (1 + \sqrt{5})/2$ . Insets show the trajectories on the Bloch sphere for the X-, Y-, and Z-axis rotations.

axes. The tetra- and octahedral groups can be implemented using only  $\pi/2$  and  $\pi$  rotations [12]. The icosahedral group requires the following rotation angles:  $\{\phi, 2\pi/5, \pi/2, 2\phi, 4\pi/5, \pi\}$ , with  $\phi$  an irrational angle from  $\tan \phi = (1 + \sqrt{5})/2$  the golden ratio. The decomposition into physical gates is shown in the Supplementary Information. The average number of physical gates per tetra-, octa- or icosahedral rotation is  $1\frac{3}{4}$ ,  $1\frac{7}{8}$ , and  $4\frac{4}{15}$ , respectively. This decomposition requires a minimal number of used angles and only one irrational angle.

The rotations are implemented in our superconducting quantum system, the Xmon transmon qubit [13]. This qubit combines full, direct axial control with a high level of coherence. Details of the device used in this experiment can be found in Ref. [8]. Rotations around the X and Y axes are achieved by applying microwave pulses. Rotations around the Z axis can be directly performed by detuning the qubit frequency, or by combining X and Y rotations. All control pulses have cosine envelopes, generated by fast (1 Gsample/sec) digital-to-analog converter boards. For XY control we generate both the in-phase and quadrature component and upconvert it to the qubit frequency using quadrature mixing, see Supplementary information and Refs. [8, 14] for more detail. For calibrating the pulse amplitudes we use the measured probability for X and Y rotations, and for Z rotations the phase as determined using quantum state tomography (Fig. 2). We minimize leakage to energy levels above the computational subspace by applying a quadrature correc-

tion [15, 16]. Subsequently, fine-tuning of the parameters is done through optimized randomized benchmarking for immediate tune-up (ORBIT) [14], reducing gate errors by approximately  $10^{-4}$  [17]. The generators of the tetrahedral and octahedral group are fully parameterized by a total of three parameters, and the generators of the icosahedral group by a total of 14 variables (Supplementary Information).

We test the gates using randomized benchmarking [8–10, 12, 18]. In essence, randomized benchmarking is equivalent to randomly rolling the die in Bloch space  $m$  times followed by a final rotation that returns it to the starting position, and then measuring the probability of success. One would like to determine the gate error averaged over all possible input states. As the gate error depends quadratically on, for example, any amount of over- or underrotation, we do not need to evaluate a continuum of input states. The average of a polynomial function of order  $t$  over the surface of a sphere can be evaluated exactly using only a finite number of points, such a group of points is a spherical  $t$ -design. For the single-qubit case, unitary designs are the group of rotations that can generate spherical designs, mapping between the points [19]. Therefore, the rotational group used in randomized benchmarking needs to be a unitary 2-design [19–22]. Moreover, unitary 2-designs depolarize any error in the computational basis. For the single-qubit case, the rotational groups which preserve Platonic solids are the 2-designs [23]. There are only three unitary 2-designs as the cube shares the same group as the octahedron (the cube and the octahedron are duals), and the dodecahedron shares the same rotations as the icosahedron (the dodecahedron and the icosahedron are duals). We have thus tested all unitary 2-designs in Bloch space.

Randomized benchmarking with 2-designs is therefore a crucial test of coherent control. The decrease of the probability of success – the sequence fidelity – with increasing sequence length is used to quantify the gate fidelity. We start by measuring a reference curve, using sequences of  $m$  random rotations. The sequence fidelity follows  $Ap^m + B$ , with variables  $A$  and  $B$  absorbing measurement and initialization errors, and  $p_{\text{ref}}$  giving the average error per rotation:  $r_{\text{ref}} = (1 - p_{\text{ref}})/2$  [18]. We then interleave a specific gate with  $m$  random rotations, the difference with the reference is a direct measure of the gate error:  $r_{\text{gate}} = (1 - p_{\text{gate}}/p_{\text{ref}})/2$ , the gate fidelity is  $F_{\text{gate}} = 1 - r_{\text{gate}}$  [24]. At each  $m$ , the data is averaged over  $k = 50$  random sequences [25].

We have performed randomized benchmarking using the tetrahedral, octahedral, and icosahedral rotational groups; the results are shown in Fig. 3. As we start by initializing the qubit in the ground state, the sequence fidelity is given by the ground state population after applying the random sequences. The traces follow an exponential decay with increasing  $m$ , as expected. We have also interleaved four gates from the tetrahedral group

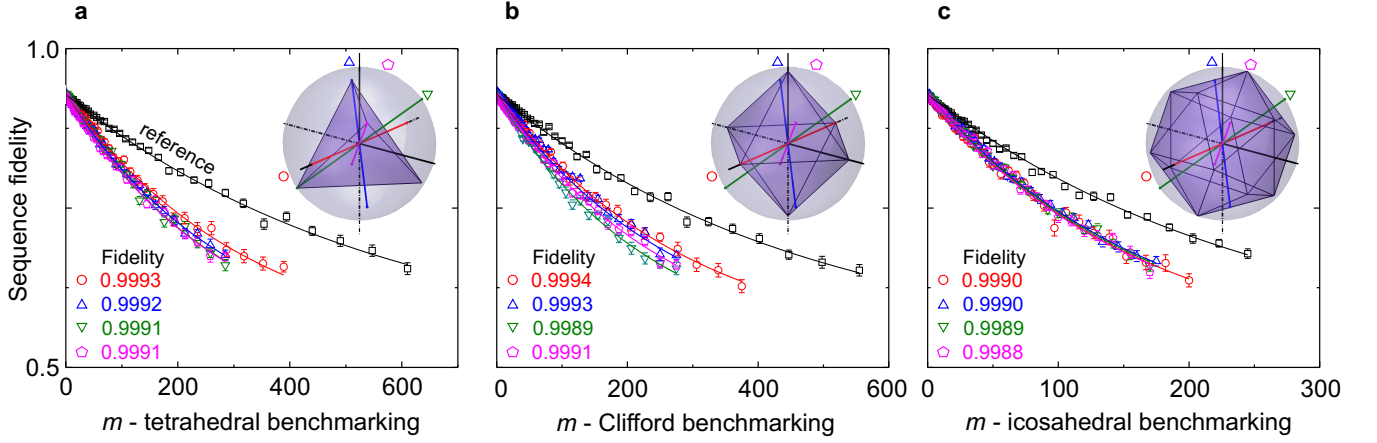


FIG. 3: **Randomized benchmarking with the (a) tetra-, (b) octa- and (c) icosahedral rotational groups.** The sequence fidelities are plotted as a function of  $m$ , the number of random rotations or sets of random rotation and interleaved gate. For each  $m$ , the fidelity is averaged over  $k = 50$  different, random sequences. From fits to the reference curves (black lines) we extract the average error per group rotation of  $r_{\text{ref},T} = 0.0009$ ,  $r_{\text{ref},C} = 0.0010$ , and  $r_{\text{ref},I} = 0.0019$ , consistent with an average physical gate fidelity of 0.9995. The rotational groups preserve Platonic solids in Bloch space, the respective solids are shown in the insets. The colored lower curves show the data when interleaving four tetrahedral rotations which are shared among all the three groups, the rotational axes are shown in the insets; the composed gates are  $X_\pi$  ( $\circ$ ),  $X_{\pi/2} Y_{\pi/2}$  ( $\Delta$ ),  $X_{-\pi/2} Y_{\pi/2}$  ( $\nabla$ ), and  $Y_{\pi/2} X_{\pi/2}$  ( $\diamond$ ). Here,  $X_{\pi/2} Y_{\pi/2}$  denotes the unitary  $R_Y(\pi/2) \cdot R_X(\pi/2) = \exp(-i\pi\sigma_Y/4) \cdot \exp(-i\pi\sigma_X/4)$ . The gate fidelities are tabulated in the figures, extracted from fits to the data (solid lines). Error bars on the data indicate the standard deviation of the mean.

(see insets for the rotational axes). These rotations are shared by all three rotational groups, allowing for a direct comparison between tetra-, octa-, and icosahedral-based randomized benchmarking. We emphasize that the interleaved gates are physically implemented in exactly the same manner.

From the reference traces, we extract an average error per group of rotations of  $r_{\text{ref},T} = 9 \cdot 10^{-4}$ ,  $r_{\text{ref},C} = 10 \cdot 10^{-4}$ ,  $r_{\text{ref},I} = 19 \cdot 10^{-4}$ . When dividing by  $1\frac{3}{4}$ ,  $1\frac{7}{8}$  or  $4\frac{4}{15}$ , these numbers consistently point to an average error of  $5 \cdot 10^{-4}$  per physical gate (single decomposed rotation around the X, Y, or Z axis). The extracted fidelities for the interleaved gates are tabulated in Fig. 3. The reference error per gate, as well as the errors for the interleaved gates, are consistent with previous measurements [8], where the average physical gate fidelity lies at 0.9994. In addition, the mean difference in error of the interleaved gates is below  $2 \cdot 10^{-4}$ , verifying that any of the groups can be used for randomized benchmarking.

With icosahedral randomized benchmarking shown to be a viable method for determining gate fidelity, we can now benchmark gates outside of the Clifford group, as shown in Fig. 4. We chose three composite gates, which are implemented using three, six, or eight physical gates. The rotational axes are highlighted in the inset. The fidelities of these gates are tabulated in the figure. These complex gates work surprisingly well: we compute the average error per physical decomposition to range between  $3 \cdot 10^{-4}$  and  $4 \cdot 10^{-4}$ , assuming that errors are small and uncorrelated. These results demonstrate that even these

complex, composite gates, can be implemented with high

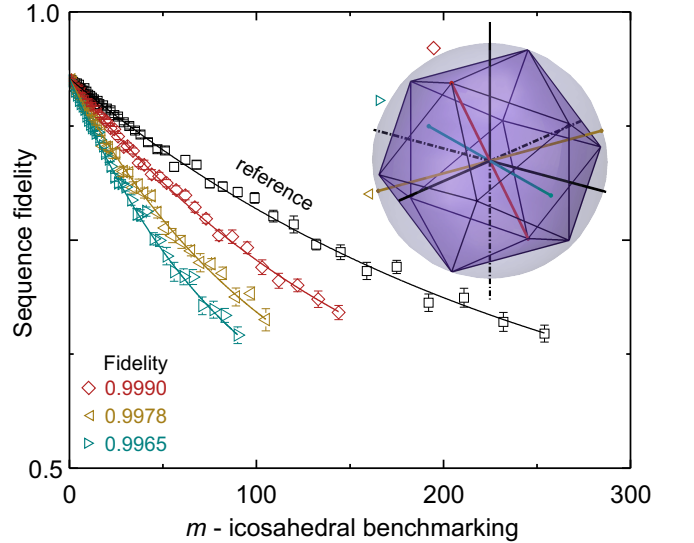


FIG. 4: **Icosahedral-based randomized benchmarking.** We have interleaved three non-Clifford gates whose axes are shown in the inset, the gates rotate around a face center, vertex or edge midpoint of the icosahedron (superimposed). The gates are composed of three, six, and eight elements. Their compositions are:  $Y_\phi X_{2\pi/5} Y_{-\phi}$  ( $\diamond$ ),  $X_\phi Z_{-2\pi/5} Y X_{2\phi} Z_{2\pi/5} X_{-\phi}$  ( $\triangleleft$ ), and  $X_\phi Z_{-2\pi/5} X_{-\phi} X_{-\pi/2} Y_{-\pi/2} X_\phi Z_{2\pi/5} X_{-\phi}$  ( $\triangleright$ ). The gate fidelities are tabulated in the figure. The average error per physical gate which makes up the interleaved gates is  $r = 3 - 4 \cdot 10^{-4}$ .

fidelity.

Apart from the first demonstrated implementation of rotational groups beyond the Clifford group, the results on icosahedral benchmarking in Figs. 3 and 4 clearly indicate that physical rotations, other than the widely used Clifford rotations, can be done with a very similar fidelity. This strongly suggests that any arbitrary rotation can be done with high fidelity. Moreover, the gate parameters can be optimized to achieve decoherence-limited performance using the method outlined in Ref. [14], providing an interpolation table for implementing any desired rotation directly, efficiently, and accurately. In addition, icosahedral benchmarking could also be used for evaluating functions of higher order, beyond gate fidelity, as the tetra-, octa-, and icosahedral rotational groups are unitary 2-, 3-, and 5-designs [26, 27].

We have shown a quantum version of rolling dice with a superconducting qubit, using gate sets inspired by the Platonic solids. Fundamentally, our work illustrates the potential of using unitaries with a finer distribution for accurate control, and provides a route for the implementation and benchmarking of non-Clifford gates. More generally, our results imply that arbitrary rotations can be done with high accuracy, allowing for complex gates and algorithms to be performed more efficiently in quantum information processing.

**Acknowledgements** R.B. acknowledges G. P. Velders for exhausting demonstrations of rolling dice. This research was funded by the Office of the Director of National Intelligence (ODNI), Intelligence Advanced Research Projects Activity (IARPA), through the Army Research Office grants W911NF-09-1-0375 and W911NF-10-1-0334. All statements of fact, opinion or conclusions contained herein are those of the authors and should not be construed as representing the official views or policies of IARPA, the ODNI, or the U.S. Government. Devices were made at the UC Santa Barbara Nanofabrication Facility, a part of the NSF-funded National Nanotechnology Infrastructure Network, and at the NanoStructures Cleanroom Facility.

**Author contributions** R.B. and J.K. designed the sample and performed the experiment. R.B. and A.V. designed the experiment. J.K., A.M., and R.B. fabricated the sample. R.B., J.K., A.V., A.G.F., A.N.K., and J.M.M. co-wrote the manuscript. All authors contributed to the fabrication process, experimental set-up, and manuscript preparation.

**Additional information** The authors declare no competing financial interests. Supplementary information accompanies this paper on [weblink to be inserted by editor]. Reprints and permissions information is available at [weblink to be inserted by editor]. Correspondence and requests for materials should be addressed to R.B. or J.M.M.

\* These authors contributed equally to this work.

- [1] Plato, Timaeus, (c. 360 BCE). Translated by B. Jowett.
- [2] Tweet, J., Cook, M., and Williams, S. *Dungeons and Dragons Player's Handbook* (Wizards of the Coast, 2000).
- [3] Hastings, M. B., Wecker D., Bauer, B., Troyer, M. Improving Quantum Algorithms for Quantum Chemistry. arXiv:1403.1539.
- [4] Lanyon, B. P., *et al.* Universal Digital Quantum Simulation with Trapped Ions. *Science* **334**, 57 (2011).
- [5] Hanneke, D., Home, J. P., Jost, J. D., Amini, J. M., Leibfried, D., and Wineland, D. J. Realization of a programmable two-qubit quantum processor. *Nature Physics* **6**, 13 - 16 (2010).
- [6] Kitaev, A. Yu. Quantum computations: algorithms and error correction. *Russ. Math. Surv.* **52** 1191 (1997).
- [7] Ross, N. J., Selinger, P. Optimal ancilla-free Clifford+T approximation of z-rotations. arXiv:1403.2975.
- [8] Barends, R. *et al.* Superconducting quantum circuits at the surface code threshold for fault tolerance. *Nature* **508**, 500-503 (2014).
- [9] Ryan, C. A., Laforest, M., & Laflamme, R. Randomized benchmarking of single-and multi-qubit control in liquid-state NMR quantum information processing. *New J. Phys.* **11**, 013034 (2009).
- [10] Harty, T. P. *et al.* High-fidelity preparation, gates, memory and readout of a trapped-ion quantum bit. arXiv:1403.1524.
- [11] Kimmel, S. *et al.* Robust Extraction of Tomographic Information via Randomized Benchmarking. *Phys. Rev. X* **4**, 011050 (2014).
- [12] Córcoles, A. D. *et al.* Process verification of two-qubit quantum gates by randomized benchmarking. *Phys. Rev. A* **87**, 030301. (2013).
- [13] Barends, R. *et al.* Coherent Josephson qubit suitable for scalable quantum integrated circuits. *Phys. Rev. Lett.* **111**, 080502 (2013).
- [14] Kelly, J. *et al.* Optimal quantum control using randomized benchmarking. arXiv:1403.0035.
- [15] Lucero, E. *et al.* Reduced phase error through optimized control of a superconducting qubit. *Phys. Rev. A* **82**, 042339 (2010).
- [16] Chow, J. M. *et al.* Implementing optimal control pulse shaping for improved single-qubit gates. *Phys. Rev. A* **82**, 040305 (2010).
- [17] We find that fine-tuning with randomized benchmarking reduces the average error from  $10 \cdot 10^{-4}$  to  $9 \cdot 10^{-4}$  per Clifford and  $20 \cdot 10^{-4}$  to  $19 \cdot 10^{-4}$  per icosahedral rotation.
- [18] Magesan, E., Gambetta, J. M., & Emerson, J. Scalable and robust randomized benchmarking of quantum processes. *Phys. Rev. Lett.* **106**, 180504 (2011).
- [19] Gross D., Audenaert K., & Eisert J. Evenly distributed unitaries: On the structure of unitary designs. *J. Math. Phys.* **48**, 052104 (2007).
- [20] Emerson, J., Alicki, R., Zyckowski, K. Scalable noise estimation with random unitary operators. *J. Opt. B: Quantum Semiclass. Opt.* **7**, S347 (2005).
- [21] Dankert, C., Cleve, R., Emerson, J., and Livine, E. Exact and Approximate Unitary 2-Designs: Constructions and Applications. *Phys. Rev. A* **80**, 012304 (2009).
- [22] Magesan, E., Gambetta, J. M., Emerson, J. Characteriz-

- ing quantum gates via randomized benchmarking. *Phys. Rev. A* **85**, 042311 (2012).
- [23] We have verified that the generated gates are a unitary 2-design: a group  $\{U_k\}_{k=1}^K$  is a 2-design if and only if  $\sum_{k,k'=1}^K |\text{Tr}(U_{k'}^\dagger U_k)|^4 / K^2 = 2$  [19].
- [24] Magesan, E. *et al.* Efficient Measurement of Quantum Gate Error by Interleaved Randomized Benchmarking. *Phys. Rev. Lett.* **109**, 080505 (2012).
- [25] Epstein, J. M., Cross, A. W., Magesan, E., Gambetta, J. M. Investigating the limits of randomized benchmarking protocols. arXiv:1308.2928.
- [26] Roy, A. and Scott, A. J. Unitary designs and codes. *Des. Codes Cryptogr.* **53**, 13-31 (2009).
- [27] A  $t$ -design is also a  $(t - 1)$ -design.

# Supplementary Information for “Rolling quantum dice with a superconducting qubit”

R. Barends,<sup>1,\*</sup> J. Kelly,<sup>1,\*</sup> A. Veitia,<sup>2</sup> A. Megrant,<sup>1</sup> A. G. Fowler,<sup>1,3</sup> B. Campbell,<sup>1</sup> Y. Chen,<sup>1</sup> Z. Chen,<sup>1</sup> B. Chiaro,<sup>1</sup> A. Dunsworth,<sup>1</sup> I.-C. Hoi,<sup>1</sup> E. Jeffrey,<sup>1</sup> C. Neill,<sup>1</sup> P. J. J. O’Malley,<sup>1</sup> J. Mutus,<sup>1</sup> C. Quintana,<sup>1</sup> P. Roushan,<sup>1</sup> D. Sank,<sup>1</sup> J. Wenner,<sup>1</sup> T. C. White,<sup>1</sup> A. N. Korotkov,<sup>2</sup> A. N. Cleland,<sup>1</sup> and John M. Martinis<sup>1</sup>

<sup>1</sup>*Department of Physics, University of California, Santa Barbara, CA 93106, USA*

<sup>2</sup>*Department of Electrical Engineering, University of California, Riverside, CA 92521, USA*

<sup>3</sup>*Centre for Quantum Computation and Communication Technology,  
School of Physics, The University of Melbourne, Victoria 3010, Australia*

## ROTATIONAL GROUPS

The tetra-, octa-, and icosahedral rotational groups are shown in Tables. S1, S2 and S3.

## PULSE CALIBRATION

The microwave pulses – the rotations around the X and Y axes – are created by generating envelopes using 1 Gsample/s digital to analog converters, and upconverting these envelopes to the qubit frequency using quadrature mixing (see Ref. [1] for the control and readout system). The room temperature electronics are calibrated by corrected the pulse from distortion using deconvolution techniques, and by correcting the quadrature mixer for gain and phase imbalances. The pulses for frequency control – the rotations around the Z axis – are generated by 1 Gsample/s digital to analog converters; non-idealities in the pulse shape from room temperature electronics are suppressed by deconvolution techniques. Non-idealities arising from stray inductance and reflections in the wiring of the cryostat are suppressed by using the qubit to measure the step response and by randomized benchmarking, see Refs. [1, 2] for details.

We then use the qubit to calibrate the pulse amplitudes, and the DRAG (derivative reduction for adiabatic gates) parameter for minimizing 2-state leakage [3, 4].

We do not calibrate the phase between a X and Y rotation using the qubit [5] as the quadrature mixer calibrations are sufficient. The pulse amplitudes for Z rotations are determined using quantum state tomography.

We use three parameters to generate the microwave pulses necessary for the tetrahedral and octahedral rotational groups (DRAG parameter, two pulse amplitudes) and 14 parameters (DRAG parameter, 13 pulse amplitudes) to generate the pulses for the icosahedral rotational group; see Table S4 for the generators.

---

\* These authors contributed equally to this work.

- [1] Barends, R. *et al.* Superconducting quantum circuits at the surface code threshold for fault tolerance. *Nature* **508**, 500-503 (2014).
- [2] Kelly, J. *et al.* Optimal quantum control using randomized benchmarking. arXiv:1403.0035.
- [3] Lucero, E. *et al.* Reduced phase error through optimized control of a superconducting qubit. *Phys. Rev. A* **82**, 042339 (2010).
- [4] Chow, J. M. *et al.* Implementing optimal control pulse shaping for improved single-qubit gates. *Phys. Rev. A* **82**, 040305 (2010).
- [5] Gustavsson, S. *et al.* Improving Quantum Gate Fidelities by Using a Qubit to Measure Microwave Pulse Distortions. *Phys. Rev. Lett.* **110**, 040502 (2013).

TABLE S1: The tetrahedral rotational group, written in terms of the physical microwave gates applied in time. Negative angles are included through opposite rotational axes.

Paulis - $\pi$	$2\pi/3$	
I	$X_{\pi/2}$	$Y_{\pi/2}$
$X_{\pi}$	$X_{\pi/2}$	$Y_{-\pi/2}$
$Y_{\pi}$	$X_{-\pi/2}$	$Y_{\pi/2}$
$Y_{\pi} X_{\pi}$	$X_{-\pi/2}$	$Y_{-\pi/2}$
	$Y_{\pi/2}$	$X_{\pi/2}$
	$Y_{\pi/2}$	$X_{-\pi/2}$
	$Y_{-\pi/2}$	$X_{\pi/2}$
	$Y_{-\pi/2}$	$X_{-\pi/2}$

TABLE S2: The octahedral rotational group – single qubit Cliffords. The Paulis and  $2\pi/3$  rotations form the tetrahedral rotational group.

Paulis - $\pi$	$2\pi/3$		$\pi/2$			Hadamard-like - $\pi$		
I	$X_{\pi/2}$	$Y_{\pi/2}$	$X_{\pi/2}$			$X_{\pi}$	$Y_{\pi/2}$	
$X_{\pi}$	$X_{\pi/2}$	$Y_{-\pi/2}$	$X_{-\pi/2}$			$X_{\pi}$	$Y_{-\pi/2}$	
$Y_{\pi}$	$X_{-\pi/2}$	$Y_{\pi/2}$	$Y_{\pi/2}$			$Y_{\pi}$	$X_{\pi/2}$	
$Y_{\pi} X_{\pi}$	$X_{-\pi/2}$	$Y_{-\pi/2}$	$Y_{-\pi/2}$			$Y_{\pi}$	$X_{-\pi/2}$	
	$Y_{\pi/2}$	$X_{\pi/2}$	$X_{-\pi/2}$	$Y_{\pi/2}$	$X_{\pi/2}$	$X_{\pi/2}$	$Y_{\pi/2}$	$X_{\pi/2}$
	$Y_{\pi/2}$	$X_{-\pi/2}$	$X_{-\pi/2}$	$Y_{-\pi/2}$	$X_{\pi/2}$	$X_{-\pi/2}$	$Y_{\pi/2}$	$X_{-\pi/2}$
	$Y_{-\pi/2}$	$X_{\pi/2}$						
	$Y_{-\pi/2}$	$X_{-\pi/2}$						

TABLE S3: The 60 icosahedral rotations, excluding the idle (I). The rotations are ordered based on their angles, and their points of intersection with the icosahedron. The edges and faces contain the Paulis and  $2\pi/3$  rotations which overlap with the tetrahedral rotational group. For the edge rotations we have used  $R_X(\phi)R_Y(\pi)R_X(-\phi) = R_X(2\phi)R_Y(\pi)$  and  $R_X(\phi)R_Z(\pi)R_X(-\phi) = R_X(2\phi)R_Z(\pi)$  to reduce the gate count.

Vertices - $2\pi/5$			Faces - $2\pi/3$								Edges - $\pi$				
$Y_\phi$	$X_{2\pi/5}$	$Y_{-\phi}$	$X_{-\pi/2}$	$Y_{-\pi/2}$						$X_\pi$					
$Y_\phi$	$X_{-2\pi/5}$	$Y_{-\phi}$	$Y_{\pi/2}$	$X_{\pi/2}$						$X_\phi Z_{2\pi/5}$	$X_\pi Z_{-2\pi/5}$	$X_{-\phi}$			
$Y_{-\phi}$	$X_{2\pi/5}$	$Y_\phi$	$X_\phi$	$Z_{-2\pi/5}$	$X_{-\phi}$	$X_{-\pi/2}$	$Y_{-\pi/2}$	$X_\phi$	$Z_{2\pi/5}$	$X_{-\phi}$	$X_\phi Z_{-2\pi/5}$	$X_\pi Z_{2\pi/5}$	$X_{-\phi}$		
$Y_{-\phi}$	$X_{-2\pi/5}$	$Y_\phi$	$X_\phi$	$Z_{-2\pi/5}$	$X_{-\phi}$	$Y_{\pi/2}$	$X_{\pi/2}$	$X_\phi$	$Z_{2\pi/5}$	$X_{-\phi}$	$X_\phi Z_{4\pi/5}$	$X_\pi Z_{-4\pi/5}$	$X_{-\phi}$		
$Z_\phi$	$Y_{2\pi/5}$	$Z_{-\phi}$	$X_\phi$	$Z_{-4\pi/5}$	$X_{-\phi}$	$X_{-\pi/2}$	$Y_{-\pi/2}$	$X_\phi$	$Z_{4\pi/5}$	$X_{-\phi}$	$X_\phi Z_{-4\pi/5}$	$X_\pi Z_{4\pi/5}$	$X_{-\phi}$		
$Z_\phi$	$Y_{-2\pi/5}$	$Z_{-\phi}$	$X_\phi$	$Z_{-4\pi/5}$	$X_{-\phi}$	$Y_{\pi/2}$	$X_{\pi/2}$	$X_\phi$	$Z_{4\pi/5}$	$X_{-\phi}$					
$Z_{-\phi}$	$Y_{2\pi/5}$	$Z_\phi$	$X_{-\pi/2}$	$Y_{\pi/2}$							$X_\phi Z_{2\pi/5}$	$Y_\pi X_{2\phi}$	$Z_{-2\pi/5} X_{-\phi}$		
$Z_{-\phi}$	$Y_{-2\pi/5}$	$Z_\phi$	$Y_{-\pi/2}$	$X_{\pi/2}$							$X_\phi Z_{-2\pi/5}$	$Y_\pi X_{2\phi}$	$Z_{2\pi/5} X_{-\phi}$		
$X_\phi$	$Z_{2\pi/5}$	$X_{-\phi}$	$X_\phi$	$Z_{2\pi/5}$	$X_{-\phi}$	$X_{-\pi/2}$	$Y_{-\pi/2}$	$X_\phi$	$Z_{-2\pi/5}$	$X_{-\phi}$	$X_\phi Z_{4\pi/5}$	$Y_\pi X_{2\phi}$	$Z_{-4\pi/5} X_{-\phi}$		
$X_\phi$	$Z_{-2\pi/5}$	$X_{-\phi}$	$X_\phi$	$Z_{2\pi/5}$	$X_{-\phi}$	$Y_{\pi/2}$	$X_{\pi/2}$	$X_\phi$	$Z_{-2\pi/5}$	$X_{-\phi}$	$X_\phi Z_{-4\pi/5}$	$Y_\pi X_{2\phi}$	$Z_{4\pi/5} X_{-\phi}$		
$X_{-\phi}$	$Z_{2\pi/5}$	$X_\phi$	$X_{\pi/2}$	$Y_{\pi/2}$							$Z_\pi$				
$X_{-\phi}$	$Z_{-2\pi/5}$	$X_\phi$	$Y_{-\pi/2}$	$X_{-\pi/2}$							$X_\phi Z_{2\pi/5}$	$Z_\pi X_{2\phi}$	$Z_{-2\pi/5} X_{-\phi}$		
			$X_\phi$	$Z_{-4\pi/5}$	$X_{-\phi}$	$X_{\pi/2}$	$Y_{\pi/2}$	$X_\phi$	$Z_{4\pi/5}$	$X_{-\phi}$	$X_\phi Z_{-2\pi/5}$	$Z_\pi X_{2\phi}$	$Z_{2\pi/5} X_{-\phi}$		
			$X_\phi$	$Z_{4\pi/5}$	$X_{-\phi}$	$X_{\pi/2}$	$Y_{\pi/2}$	$X_\phi$	$Z_{-4\pi/5}$	$X_{-\phi}$	$X_\phi Z_{4\pi/5}$	$Z_\pi X_{2\phi}$	$Z_{-4\pi/5} X_{-\phi}$		
			$X_\phi$	$Z_{4\pi/5}$	$X_{-\phi}$	$Y_{-\pi/2}$	$X_{-\pi/2}$	$X_\phi$	$Z_{-4\pi/5}$	$X_{-\phi}$	$X_\phi Z_{-4\pi/5}$	$Z_\pi X_{2\phi}$	$Z_{4\pi/5} X_{-\phi}$		
			$X_\phi$	$Z_{2\pi/5}$	$X_{-\phi}$	$X_{\pi/2}$	$Y_{\pi/2}$	$X_\phi$	$Z_{-2\pi/5}$	$X_{-\phi}$					
			$X_\phi$	$Z_{2\pi/5}$	$X_{-\phi}$	$Y_{-\pi/2}$	$X_{-\pi/2}$	$X_\phi$	$Z_{-2\pi/5}$	$X_{-\phi}$					
			$X_{\pi/2}$	$Y_{-\pi/2}$											
			$Y_{\pi/2}$	$X_{-\pi/2}$											
			$X_\phi$	$Z_{-4\pi/5}$	$X_{-\phi}$	$X_{\pi/2}$	$Y_{\pi/2}$	$X_\phi$	$Z_{4\pi/5}$	$X_{-\phi}$					
			$X_\phi$	$Z_{-4\pi/5}$	$X_{-\phi}$	$Y_{-\pi/2}$	$X_{-\pi/2}$	$X_\phi$	$Z_{4\pi/5}$	$X_{-\phi}$					
			$X_\phi$	$Z_{4\pi/5}$	$X_{-\phi}$	$X_{\pi/2}$	$Y_{\pi/2}$	$X_\phi$	$Z_{-4\pi/5}$	$X_{-\phi}$					
			$X_\phi$	$Z_{4\pi/5}$	$X_{-\phi}$	$Y_{-\pi/2}$	$X_{-\pi/2}$	$X_\phi$	$Z_{-4\pi/5}$	$X_{-\phi}$					
			$X_\phi$	$Z_{2\pi/5}$	$X_{-\phi}$	$X_{\pi/2}$	$Y_{\pi/2}$	$X_\phi$	$Z_{-2\pi/5}$	$X_{-\phi}$					
			$X_\phi$	$Z_{2\pi/5}$	$X_{-\phi}$	$Y_{-\pi/2}$	$X_{-\pi/2}$	$X_\phi$	$Z_{-2\pi/5}$	$X_{-\phi}$					
			$X_{\pi/2}$	$Y_{-\pi/2}$											
			$Y_{\pi/2}$	$X_{-\pi/2}$											
			$X_\phi$	$Z_{-4\pi/5}$	$X_{-\phi}$	$X_{\pi/2}$	$Y_{\pi/2}$	$X_\phi$	$Z_{4\pi/5}$	$X_{-\phi}$					
			$X_\phi$	$Z_{-4\pi/5}$	$X_{-\phi}$	$Y_{-\pi/2}$	$X_{-\pi/2}$	$X_\phi$	$Z_{4\pi/5}$	$X_{-\phi}$					
			$X_\phi$	$Z_{4\pi/5}$	$X_{-\phi}$	$X_{\pi/2}$	$Y_{\pi/2}$	$X_\phi$	$Z_{-4\pi/5}$	$X_{-\phi}$					
			$X_\phi$	$Z_{4\pi/5}$	$X_{-\phi}$	$Y_{-\pi/2}$	$X_{-\pi/2}$	$X_\phi$	$Z_{-4\pi/5}$	$X_{-\phi}$					
			$X_\phi$	$Z_{2\pi/5}$	$X_{-\phi}$	$X_{\pi/2}$	$Y_{\pi/2}$	$X_\phi$	$Z_{-2\pi/5}$	$X_{-\phi}$					
			$X_\phi$	$Z_{2\pi/5}$	$X_{-\phi}$	$Y_{-\pi/2}$	$X_{-\pi/2}$	$X_\phi$	$Z_{-2\pi/5}$	$X_{-\phi}$					
			$X_{\pi/2}$	$Y_{-\pi/2}$											
			$Y_{\pi/2}$	$X_{-\pi/2}$											

TABLE S4: Generators of the tetra-, octa-, and icosahedral rotational groups, excluding the idle. The generators are listed in terms of shared pulse amplitude parameter. Including the DRAG parameter, we use a total of three parameters to generate the tetra-, and octahedral rotational group (DRAG parameter, pulse amplitude parameter for  $X_\pi$  and  $Y_\pi$ , pulse amplitude parameter for  $X_{\pi/2}$ ,  $X_{-\pi/2}$ ,  $Y_{\pi/2}$ , and  $Y_{-\pi/2}$ ), and a total of 14 parameters to generate the icosahedral rotational group. The duration of the idle and each of the X and Y gates is 12 ns, and each Z gate is 10 ns.

Rotational group	Generators
Tetrahedral, octahedral, and icosahedral	$X_\pi, Y_\pi$
	$X_{\pi/2}, X_{-\pi/2}, Y_{\pi/2}, Y_{-\pi/2}$
Icosahedral	$X_{2\pi/5}, X_{-2\pi/5}, Y_{2\pi/5}, Y_{-2\pi/5}$
	$X_{4\pi/5}, X_{-4\pi/5}, Y_{4\pi/5}, Y_{-4\pi/5}$
	$X_\phi, Y_\phi, X_{-\phi}, Y_{-\phi}$
	$X_{2\phi}$
	$Z_{2\pi/5}$
	$Z_{-2\pi/5}$
	$Z_\phi$
	$Z_{-\phi}$
	$Z_{4\pi/5}$
	$Z_{-4\pi/5}$
	$Z_\pi$